Relativistic description of the semileptonic decays of bottom mesons

R. N. Faustov,[1,*] V. O. Galkin,[1,†] and Xian-Wei Kang[2,3,‡]

[1]*Federal Research Center "Computer Science and Control", Russian Academy of Sciences, Vavilov Street 40, 119333 Moscow, Russia*

[2]*Key Laboratory of Beam Technology of the Ministry of Education, College of Nuclear Science and Technology, Beijing Normal University, Beijing 100875, China*

[3]*Institute of Radiation Technology, Beijing Academy of Science and Technology, Beijing 100875, China*

(Received 22 June 2022; accepted 5 July 2022; published 12 July 2022)

The form factors of the semileptonic B, B_s, and B_c meson decays are calculated in the framework of the relativistic quark model based on the quasipotential approach in QCD. They are expressed through the overlap integrals of the meson wave function. All relativistic effects are consistently taken into account. The momentum transfer q^2 behavior of form factors is determined in the whole accessible kinematical range. We do not use any extrapolations, heavy quark $1/m_Q$ expansion, or model assumptions about the shape of form factors. Convenient analytic expressions of the form factors are given, which very accurately reproduce the numerical results of our calculation. On the basis of these form factors and helicity formalism, the differential and total branching fractions of various semileptonic decays of bottom meson are calculated. The mean values of the forward-backward asymmetry $\langle A_{\rm FB}\rangle$, lepton-side convexity parameter $\langle C_F^\ell\rangle$, longitudinal $\langle P_L^\ell\rangle$ and transverse $\langle P_T^\ell\rangle$ polarization of the charged lepton, and the longitudinal polarization fraction $\langle F_L\rangle$ for final-state vector meson are also evaluated. We present a detailed comparison of the obtained predictions with the calculations based on the covariant light-front quark model and confront them to available lattice QCD and experimental data. It is found that although both models predict close values of the total branching fractions, the differential distributions and forward-backward asymmetry and polarization parameters differ significantly, especially for the heavy-to-light semileptonic decays. We identify observables which measurement can help to discriminate between models.

DOI: 10.1103/PhysRevD.106.013004

I. INTRODUCTION

The semileptonic decays are the main source of the determination of the Cabibbo-Kobayashi-Maskawa (CKM) matrix elements which are the fundamental parameters of the Standard Model (SM). The important feature of SM is the universality of the electroweak coupling to all the three generations of fermions, which leads to a lepton flavor universality. As a result the lepton flavor symmetry between semileptonic decay rates involving different lepton flavors arise when the charged lepton mass contributions to decay amplitudes and phase space are taken into account. Thus investigation of semileptonic decays can be used to test SM. Any deviations from the CKM matrix unitarity constraints and lepton flavor universality will be a signal of the so-called new physics. There is a longstanding tension between the values of $|V_{cb}|$ and $|V_{ub}|$ extracted from experimental data [1] on exclusive and inclusive semileptonic decays (for a recent review see Ref. [2]). Some hints of the possible lepton flavor violation, due to the anomalously high rates for semileptonic $b \to c\tau\nu_\tau$ compared to SM predictions, were also reported (see, e.g., Ref. [3] for a recent review). However, the most recent experimental data tend to decrease these deviations.

The experimental and theoretical studies of semileptonic decays of bottom mesons, which are governed by $b \to c$ and $b \to u$ quark transitions, are important for the determination of the CKM matrix elements $|V_{cb}|$ and $|V_{ub}|$. The semileptonic decays of B_c meson to B_s and B mesons proceed through $c \to s$ and $c \to d$ quark transitions, and thus are proportional to the CKM matrix elements $|V_{cs}|$ and $|V_{cd}|$. The main theoretical difficulty in considering exclusive semileptonic decays of bottom mesons is related to the calculation of the form factors, which parametrize the hadronic matrix elements, since the lepton part can be easily calculated by the standard methods. It is important to reliably determine the momentum transfer squared q^2

*faustov@ccas.ru
†galkin@ccas.ru
‡xwkang@bnu.edu.cn

behavior of these form factors in the whole accessible kinematical range, since differential distributions are very sensitive to it. This is especially important for heavy-to-light decays since they have a very broad q^2 range. Most of the theoretical approaches determine these form factors at some particular kinematical points or in the limited q^2 range and then extrapolate them using some model parametrizations. For example, light cone sum rules [4] calculate form factors at the maximum recoil point of the final meson $q^2 = 0$ (the small electron mass is neglected), while in lattice QCD calculations the high q^2 region is investigated (for a review see, e.g., Ref. [5] and references therein). And also in most considerations of heavy-to-heavy ($B \to D^{(*)}$) semileptonic decays the heavy quark $1/m_Q$ expansion is employed. Some very recent works on the semileptonic bottom meson decay are in, e.g., [6–8], where it is interesting that in Ref. [6] both the space- and timelike momentum transfer regions are considered.

In the present paper we use the relativistic quark model based on the quasipotential approach in QCD for the calculations of the bottom meson transition form factors in the whole accessible kinematical range. The comprehensive account of the relativistic effects allows us to achieve this goal without any expansions and extrapolations. On this basis we calculated semileptonic decay branching fractions of bottom mesons as well as differential distributions, forward-backward (FB) asymmetry and polarization parameters. A similar approach was recently used by us for consideration of the D meson semileptonic decays [9]. We present also the detailed comparison of our predictions with the results of the other popular quark model—the covariant light-front quark model (CLFQM) [10,11] and identify observables which measurement can help to discriminate between models. Model predictions are also compared with available data from the experiment and lattice QCD.

II. RELATIVISTIC QUARK MODEL

We use the relativistic quark model (RQM) based on the quasipotential approach to calculate the form factors parametrizing the matrix elements of the weak B, B_s, and B_c meson decays. In this model a meson M is considered as a quark-antiquark bound state described by the wave function Ψ_M, which satisfies the three-dimensional relativistically invariant Schrödinger-type quasipotential equation [12]

$$\left(\frac{b^2(M)}{2\mu_R} - \frac{\mathbf{p}^2}{2\mu_R}\right)\Psi_M(\mathbf{p}) = \int \frac{d^3q}{(2\pi)^3} V(\mathbf{p},\mathbf{q};M)\Psi_M(\mathbf{q}), \quad (1)$$

where

$$b^2(M) = \frac{[M^2 - (m_1+m_2)^2][M^2 - (m_1-m_2)^2]}{4M^2} \quad (2)$$

and

$$\mu_R = \frac{M^4 - (m_1^2 - m_2^2)^2}{4M^3} \quad (3)$$

are the relative momentum squared on mass shell in the center of mass system and the relativistic reduced mass, respectively. Here M is the meson mass, $m_{1,2}$ are the quark masses, and $\mathbf{p}$ is their relative momentum.

The kernel of this equation $V(\mathbf{p},\mathbf{q};M)$ is the quark-antiquark interaction quasipotential. In RQM it is constructed [12] with the help of the QCD-motivated off-mass-shell scattering amplitude projected on the positive energy states. The effective quark-antiquark interaction is chosen as the sum of the one-gluon exchange potential, which dominates at short distances, and the long range confining interaction linearly increasing with a quark separation, which dominates at large distances. The Lorentz-structure of the confining interaction is assumed to be the mixture of the vector and scalar terms with the mixing coefficient ϵ. It is also assumed that the vertex of the vector confining interaction $\Gamma_\mu(\mathbf{k})$ with $\mathbf{k} = \mathbf{p} - \mathbf{q}$ contains both Dirac and Pauli terms

$$\Gamma_\mu(\mathbf{k}) = \gamma_\mu + \frac{i\kappa}{2m}\sigma_{\mu\nu}k^\nu, \quad (4)$$

thus, introducing the long-range anomalous chromomagnetic quark moment κ. In the nonrelativistic limit this quasipotential reduces to the standard Cornell potential

$$V(r) = -\frac{4}{3}\frac{\alpha_s}{r} + Ar + B, \quad (5)$$

where α_s is the QCD coupling constant. Therefore, our quasipotential can be considered as its relativistic generalization, which takes into account both spin-independent and spin-dependent contributions. Its explicit form can be found in Ref. [13].

All parameters of the model were fixed from previous considerations of meson properties [12–15]. The constituent quark masses $m_u = m_d = 0.33$ GeV, $m_s = 0.5$ GeV, $m_c = 1.55$ GeV and $m_b = 4.88$ GeV and parameters of confining potential $A = 0.18$ GeV^2 and $B = -0.30$ GeV have values standard for the quark models. Our extra parameters: the mixing coefficient of vector and scalar confining potentials is $\epsilon = -1$ and the long-range anomalous chromomagnetic moment is $\kappa = -1$. For the chosen value of κ, the long range chromomagnetic interaction, which is proportional to $(1+\kappa)$, vanishes in accord with the flux tube model.

The spectroscopy of the heavy [15], heavy-light [14] and light [13] mesons was considered previously. The quasipotential equation (1) with the complete relativistic quasipotential was solved numerically. Masses of ground and excited mesons were found in good agreement with

available experimental data. The numerical wave functions of the meson states were obtained. Here we apply these wave functions for the calculations of the weak decay form factors of B, B_s, and B_c mesons.

In the quasipotential approach the matrix element of the weak current $J^W_\mu = \bar{q}\gamma_\mu(1-\gamma_5)b$ $(q = u, c)$ between initial $(B = B, B_s, B_c)$ and final $(F = D^{(*)}, D_s^{(*)}, \pi, \rho, \eta, \eta', \omega, K^{(*)}, \eta_c, J/\psi)$ meson states is expressed as [16–18]

$$\langle F(p_F)|J^W_\mu|B(p_B)\rangle = \int \frac{d^3p d^3q}{(2\pi)^6}\bar{\Psi}_{F\mathbf{p}_F}(\mathbf{p})\Gamma_\mu(\mathbf{p},\mathbf{q})\Psi_{B\mathbf{p}_B}(\mathbf{q}), \tag{6}$$

where p_B and p_F are the initial and final meson momenta, respectively. The wave functions $\Psi_{M\mathbf{p}_M}$ of the initial $(M = B)$ and final $(M = F)$ mesons are projected on the positive energy states and boosted to the moving reference frame with the three-momentum $\mathbf{p}_M$. The wave function of the moving meson $\Psi_{M\mathbf{p}_M}$ is connected with the wave function in the rest reference frame $\Psi_{M\mathbf{0}}$ by the transformation [16]

$$\Psi_{M\mathbf{p}_M}(\mathbf{p}) = D^{1/2}_q(R^W_{L_{\mathbf{p}_M}})D^{1/2}_{\bar{q}_s}(R^W_{L_{\mathbf{p}_M}})\Psi_{M\mathbf{0}}(\mathbf{p}), \tag{7}$$

where q and $\bar{q}_s$ are the active quark and spectator antiquark, respectively. R^W is the Wigner rotation, $L_{\mathbf{p}_M}$ is the Lorentz boost from the meson rest frame to a moving one, and $D^{1/2}(R)$ is the spin rotation matrix

$$\begin{pmatrix} 1 & 0 \\ 0 & 1 \end{pmatrix} D^{1/2}_q(R^W_{L_{\mathbf{p}_M}}) = S^{-1}(\mathbf{p}_q)S(\mathbf{p}_M)S(\mathbf{p}),$$

with

$$S(\mathbf{p}) = \sqrt{\frac{\epsilon(\mathbf{p})+m}{2m}}\left(1 + \frac{\boldsymbol{\alpha}\cdot\mathbf{p}}{\epsilon(\mathbf{p})+m}\right),$$

with $\boldsymbol{\alpha} = \gamma_0\boldsymbol{\gamma}$ being the product of the Dirac matrices, and m is the corresponding quark or meson mass.

The vertex function of the W-boson interaction consists of two terms $\Gamma_\mu(\mathbf{p},\mathbf{q}) = \Gamma^{(1)}_\mu(\mathbf{p},\mathbf{q}) + \Gamma^{(2)}_\mu(\mathbf{p},\mathbf{q})$. The first term corresponds to the impulse approximation, where there is no interaction between the active quark and spectator antiquark. Thus it contains the $\delta(\mathbf{p}_s - \mathbf{q}_s)$ function which is responsible for the momentum conservation on the spectator $\bar{q}_s$ line. The second term is the consequence of the projection on the positive energy states and takes into account interaction of the negative energy part of the active quark with the spectator antiquark, so-called Z-diagrams. Thus, this term includes the $q\bar{q}$ interaction quasipotentials $V(\mathbf{p},\mathbf{q};M)$ and the negative-energy parts of the quark propagators. The corresponding diagrams and explicit expressions for the vertex functions $\Gamma^{(1),(2)}_\mu(\mathbf{p},\mathbf{q})$ are given in Ref. [16].

It is convenient to express the weak decay matrix element, Eq. (6), in the form of the overlap integral of the meson wave functions. It can be easily done for the leading contribution $\Gamma^{(1)}_\mu(\mathbf{p},\mathbf{q})$, since it contains the δ-function, which allows one to take one of the integrations in Eq. (6). The second contribution $\Gamma^{(2)}_\mu(\mathbf{p},\mathbf{q})$ is more complicated. Instead of the δ-function it contains the quasipotential $V(\mathbf{p},\mathbf{q};M)$ with the nontrivial Lorentz-structure. However, it is possible to use the quasipotential equation to take off one of the integrations in Eq. (6) and thus to get the desired form of the matrix elements (for details see Ref. [16]). As a result this contribution is proportional to the ratio of the meson binding energy to the energy of the active quark. Therefore, it is indeed the subleading contribution. It turns out to be rather small for all heavy-to-heavy meson weak decays. For the heavy-to-light decays its contribution is suppressed for large recoils of the final meson due to the large energy of the final active quark but becomes important at small recoils.

III. FORM FACTORS OF SEMILEPTONIC DECAYS

The hadronic matrix element of the weak current J^W_μ between meson states is usually parametrized by the following set of invariant form factors.

(i) For B transition to the pseudoscalar P meson (where B symbolically denotes either B, B_s, or B_c)

$$\begin{aligned}\langle P(p_P)|\bar{q}\gamma^\mu b|B(p_B)\rangle &= f_+(q^2)\left[p^\mu_B + p^\mu_P - \frac{M^2_B - M^2_P}{q^2}q^\mu\right] + f_0(q^2)\frac{M^2_B - M^2_P}{q^2}q^\mu,\\ \langle P(p_P)|\bar{q}\gamma^\mu\gamma_5 b|B(p_B)\rangle &= 0,\end{aligned} \tag{8}$$

(ii) For B transition to the vector V meson

$$\begin{aligned}\langle V(p_V)|\bar{q}\gamma^\mu b|B(p_B)\rangle &= \frac{2iV(q^2)}{M_B + M_V}\epsilon^{\mu\nu\rho\sigma}\epsilon^*_\nu p_{B\rho}p_{V\sigma},\\ \langle V(p_V)|\bar{q}\gamma^\mu\gamma_5 b|B(p_B)\rangle &= 2M_V A_0(q^2)\frac{\epsilon^*\cdot q}{q^2}q^\mu + (M_B + M_V)A_1(q^2)\left(\epsilon^{*\mu} - \frac{\epsilon^*\cdot q}{q^2}q^\mu\right)\\ &\quad - A_2(q^2)\frac{\epsilon^*\cdot q}{M_B + M_V}\left[p^\mu_B + p^\mu_V - \frac{M^2_B - M^2_V}{q^2}q^\mu\right],\end{aligned} \tag{9}$$

here $q = p_B - p_F$ $(F = P,\ V)$. At the maximum recoil point $(q^2 = 0)$ these form factors satisfy the following conditions:

$$f_+(0) = f_0(0),$$
$$A_0(0) = \frac{M_B + M_V}{2M_V} A_1(0) - \frac{M_B - M_V}{2M_V} A_2(0).$$

These form factors are calculated in RQM with the systematic consideration of all relativistic effects as described in the previous section. Relativistic transformations of the meson wave functions from the rest reference frame to the moving one, cf. Eq. (7), as well as relativistic contributions from the intermediate negative-energy states are consistently taken into account. The explicit expressions for these form factors in terms of the overlap integrals of initial and final meson wave functions can be found in Ref. [19]. It was shown previously [16,20], that applying the heavy quark expansion to these expressions for the case of heavy-to-heavy meson transitions, it is possible to reproduce the model independent expressions of heavy quark effective theory at leading, first and second order in $1/m_Q$ and obtain expressions for the corresponding Isgur-Wise functions. In the present paper we do not use the heavy quark expansion and calculate all form factors nonperturbatively employing relativistic meson wave functions. Such approach allows us to reliably determine the momentum transfer squared (q^2) dependence of these form factors in the whole accessible kinematic range [16–18]. The obtained numerical results can be approximated with high accuracy by the following expressions:

(i) for the form factors $f_+(q^2), V(q^2), A_0(q^2)$

$$F(q^2) = \frac{F(0)}{(1 - \frac{q^2}{M^2})(1 - \sigma_1 \frac{q^2}{M_1^2} + \sigma_2 \frac{q^4}{M_1^4})}, \quad (10)$$

(ii) for the form factors $f_0(q^2), A_1(q^2), A_2(q^2)$

$$F(q^2) = \frac{F(0)}{(1 - \sigma_1 \frac{q^2}{M_1^2} + \sigma_2 \frac{q^4}{M_1^4})}, \quad (11)$$

where the masses M and M_1 are given in Table I. For the decays governed by the CKM favored $b \to c$ transitions, for pole masses M we use the masses of the intermediate vector B_c^* mesons for the form factors $f_+(q^2), V(q^2)$ and of the pseudoscalar B_c for the form factor $A_0(q^2)$. While for the decays governed by the CKM suppressed $b \to u$ transitions, masses of the intermediate B^* and B mesons are used, respectively. For $B_c \to B_s$ decays governed by the CKM favored $c \to s$ transitions and $B_c \to B$ decays governed by the CKM suppressed $c \to d$ transitions, for pole masses M we use the respective masses of vector D_s^* and D^* mesons and pseudoscalar D_s and D mesons. The values of form factors $F(0)$, $F(q^2_{\rm max})$ and fitted parameters $\sigma_{1,2}$ for

TABLE I. Masses in parametrizations of the weak decay form factors of B, B_s, and B_c mesons, cf. Eqs. (10) and (11).

Quark transition	Decay	M_1 (GeV)	M (GeV)	
			$f_+(q^2), V(q^2)$	$A_0(q^2)$
$b \to c$	$B \to D(D^*)$ $B_s \to D_s(D_s^*)$ $B_c \to \eta_c(J/\psi)$	6.332	6.332	6.277
$b \to u$	$B \to \pi(\rho)$ $B \to \eta^{(\prime)}(\omega)$ $B_s \to K(K^*)$ $B_c \to D(D^*)$	5.325	5.325	5.280
$c \to s$	$B_c \to B_s(B_s^*)$	6.332	2.112	1.968
$c \to d$	$B_c \to B(B^*)$	6.332	2.010	1.870

TABLE II. Form factors of the weak B and B_s meson transitions in RQM.

Transition	Form factor	$F(0)$	$F(q^2_{\rm max})$	σ_1	σ_2
$B \to D$	f_+	0.696	1.24	1.288	1.943
	f_0	0.696	0.82	0.731	0.736
$B \to D^*$	V	0.915	1.38	0.647	1.100
	A_0	0.814	1.21	0.645	1.300
	A_1	0.730	0.83	0.571	0.457
	A_2	0.627	1.02	0.719	−2.690
$B \to \pi$	f_+	0.217	10.9	0.378	−0.410
	f_0	0.217	1.32	−0.501	−1.50
$B \to \rho$	V	0.295	2.80	0.875	0
	A_0	0.231	2.19	0.796	−0.055
	A_1	0.269	0.439	0.540	0
	A_2	0.282	1.92	1.34	0.210
$B \to \eta$	f_+	0.194	2.75	0.181	−0.835
	f_0	0.194	0.52	0.458	−0.424
$B \to \eta'$	f_+	0.187	1.34	0.637	−0.396
	f_0	0.187	0.32	0.996	0.565
$B \to \omega$	V	0.263	2.47	0.894	0.021
	A_0	0.244	1.96	0.826	0.084
	A_1	0.232	0.46	0.676	−0.032
	A_2	0.229	0.96	1.453	0.539
$B_s \to D_s$	f_+	0.663	1.23	1.375	1.877
	f_0	0.663	0.87	1.018	0.705
$B_s \to D_s^*$	V	0.925	1.48	0.965	1.534
	A_0	0.625	1.03	0.457	−0.710
	A_1	0.668	0.82	0.913	0.766
	A_2	0.723	1.09	1.349	0.230
$B_s \to K$	f_+	0.284	5.42	−0.370	−1.41
	f_0	0.284	0.459	−0.072	−0.651
$B_s \to K^*$	V	0.291	3.06	−0.516	−2.10
	A_0	0.289	2.10	−0.383	−1.58
	A_1	0.287	0.581	0	−1.06
	A_2	0.286	0.953	1.05	0.074

TABLE III. Form factors of the weak B_c meson transitions in RQM.

Transition	Form factor	$F(0)$	$F(q^2_{\rm max})$	σ_1	σ_2
$B_c \to \eta_c$	f_+	0.431	1.09	2.103	1.510
	f_0	0.431	0.93	2.448	1.700
$B_c \to J/\psi$	V	0.513	1.32	1.815	−0.320
	A_0	0.360	0.93	2.335	1.721
	A_1	0.459	0.89	2.415	1.929
	A_2	0.653	1.33	2.765	2.939
$B_c \to D$	f_+	0.081	3.21	2.167	1.203
	f_0	0.081	0.63	2.455	1.729
$B_c \to D^*$	V	0.125	3.11	2.247	1.346
	A_0	0.035	0.99	1.511	0.175
	A_1	0.054	0.78	2.595	1.784
	A_2	0.071	1.25	2.800	2.073
$B_c \to B_s$	f_+	0.524	0.990	10.91	−292.1
	f_0	0.524	0.822	19.47	92.36
$B_c \to B_s^*$	V	2.08	4.78	18.88	−372.8
	A_0	0.431	0.736	12.23	−141.5
	A_1	0.518	0.850	19.11	−103.6
	A_2	1.62	2.02	17.47	366.5
$B_c \to B$	f_+	0.394	0.969	4.970	−550.2
	f_0	0.394	0.680	19.92	117.7
$B_c \to B^*$	V	1.84	4.79	11.48	−477.1
	A_0	0.380	0.906	11.32	−349.7
	A_1	0.457	0.822	19.55	−2.685
	A_2	1.33	1.92	22.82	407.6

the weak decays of B and B_s mesons are given in Table II and of the B_c meson in Table III. We estimate the uncertainties of the calculated form factors to be less than 5%.

IV. SEMILEPTONIC DECAYS OF BOTTOM MESONS

The differential distribution of the B meson semileptonic decay to the final ground state pseudoscalar or vector meson ($F = P, V$) has the following expression in terms of the helicity components [11,21]:

$$\frac{d\Gamma(B\to F\ell^+\nu_\ell)}{dq^2 d(\cos\theta)} = \frac{G_F^2}{(2\pi)^3}|V_{q_1q_2}|^2\frac{\lambda^{1/2}q^2}{64M_B^3}\left(1-\frac{m_\ell^2}{q^2}\right)^2 \times\left[(1+\cos^2\theta)\mathcal{H}_U+2\sin^2\theta\mathcal{H}_L+2\cos\theta\mathcal{H}_P +\frac{m_\ell^2}{q^2}(\sin^2\theta\mathcal{H}_U+2\cos^2\theta\mathcal{H}_L+2\mathcal{H}_S-4\cos\theta\mathcal{H}_{SL})\right], \quad (12)$$

where $V_{q_1q_2}$ is the corresponding CKM matrix element, $\lambda\equiv\lambda(M_B^2,M_F^2,q^2)=M_B^4+M_F^4+q^4-2(M_B^2M_F^2+M_F^2q^2+M_B^2q^2)$, m_ℓ is the lepton mass ($\ell = e,\ \mu,\ \tau$), and the polar angle θ is the angle between the momentum of the charged lepton in the rest frame of the intermediate W-boson and the direction opposite to the final F meson momentum in the rest frame of the initial B meson. $\mathcal{H}_I$ ($I = U, L, P, S, SL$) are the bilinear combinations of the helicity components of the hadronic tensor [11,21]:

$$\mathcal{H}_U=|H_+|^2+|H_-|^2,\quad \mathcal{H}_L=|H_0|^2,\quad \mathcal{H}_P=|H_+|^2-|H_-|^2,$$
$$\mathcal{H}_S=|H_t|^2,\quad \mathcal{H}_{SL}=\Re(H_0H_t^\dagger), \quad (13)$$

where the helicity amplitudes H_i ($i = +, -, 0, t$) are the following combinations of invariant form factors considered in the previous section.

(i) For B to the pseudoscalar P meson transitions, the helicity amplitudes are given by

$$H_\pm = 0,\qquad H_0=\frac{\lambda^{1/2}}{\sqrt{q^2}}f_+(q^2),$$
$$H_t=\frac{1}{\sqrt{q^2}}(M_B^2-M_P^2)f_0(q^2). \quad (14)$$

(ii) For B to the vector V meson transitions, the helicity amplitudes are the following

$$H_\pm(q^2)=(M_B+M_V)A_1(q^2)\mp\frac{\lambda^{1/2}}{M_B+M_V}V(q^2),$$
$$H_0(q^2)=\frac{1}{2M_V\sqrt{q^2}}\left[(M_B+M_V)(M_B^2-M_V^2-q^2)A_1(q^2)-\frac{\lambda}{M_B+M_V}A_2(q^2)\right],$$
$$H_t=\frac{\lambda^{1/2}}{\sqrt{q^2}}A_0(q^2). \quad (15)$$

The expression (12), normalized by the differential decay distribution integrated over $\cos\theta$

$$d\Gamma/dq^2\equiv\frac{d\Gamma(B\to F\ell^+\nu_\ell)}{dq^2} =\frac{G_F^2}{(2\pi)^3}|V_{q_1q_2}|^2\frac{\lambda^{1/2}q^2}{24M_B^3}\left(1-\frac{m_\ell^2}{q^2}\right)^2\mathcal{H}_{\rm total}, \quad (16)$$

can be rewritten as

$$\frac{1}{d\Gamma/dq^2}\frac{d\Gamma(B\to F\ell^+\nu_\ell)}{dq^2 d(\cos\theta)} = \frac{1}{2}\left[1-\frac{1}{3}C_F^\ell(q^2)\right] + A_{\rm FB}(q^2)\cos\theta + \frac{1}{2}C_F^\ell(q^2)\cos^2\theta. \quad (17)$$

Here $\mathcal{H}_{\rm total}$ is the total helicity structure

$$\mathcal{H}_{\rm total} = (\mathcal{H}_U+\mathcal{H}_L)\left(1+\frac{m_\ell^2}{2q^2}\right)+\frac{3m_\ell^2}{2q^2}\mathcal{H}_S. \quad (18)$$

In the differential decay distribution, Eq. (17), $A_{\rm FB}(q^2)$ is the FB asymmetry defined by

$$A_{\rm FB}(q^2) = \frac{3}{4}\frac{\mathcal{H}_P - 2\frac{m_\ell^2}{q^2}\mathcal{H}_{SL}}{\mathcal{H}_{\rm total}}, \quad (19)$$

and $C_F^\ell(q^2)$ is the lepton-side convexity parameter, which is the second derivative of the distribution (17) over $\cos\theta$, given by

$$C_F^\ell(q^2) = \frac{3}{4}\left(1-\frac{m_\ell^2}{q^2}\right)\frac{\mathcal{H}_U - 2\mathcal{H}_L}{\mathcal{H}_{\rm total}}. \quad (20)$$

The longitudinal polarization of the final charged lepton ℓ is defined as the ratio of the longitudinally polarized decay distribution to the unpolarized decay distribution, Eq. (16) [11,21]:

$$P_L^\ell(q^2) = \frac{1}{d\Gamma/dq^2}\frac{d\Gamma(s_L)}{dq^2} = \frac{(\mathcal{H}_U+\mathcal{H}_L)\left(1-\frac{m_\ell^2}{2q^2}\right)-\frac{3m_\ell^2}{2q^2}\mathcal{H}_S}{\mathcal{H}_{\rm total}}, \quad (21)$$

and its transverse polarization is given by [11,21]

$$P_T^\ell(q^2) = \frac{1}{d\Gamma/dq^2}\frac{d\Gamma(s_T)}{dq^2} = -\frac{3\pi m_\ell}{8\sqrt{q^2}}\frac{\mathcal{H}_P+2\mathcal{H}_{SL}}{\mathcal{H}_{\rm total}}, \quad (22)$$

where $s_{L(T)}$ is the longitudinal (transverse) polarization vector of the final lepton ℓ, which is parallel (perpendicular) to the lepton momentum.

For the B decays to the vector V meson, which then decays to two pseudoscalar mesons $V\to P_1P_2$, the differential distribution in the angle θ^*, defined as the polar angle between the vector meson V momentum in the B meson rest frame and the pseudoscalar meson P_1 momentum in the rest frame of the vector meson V, is given by [11,21]

$$\frac{1}{d\Gamma/dq^2}\frac{d\Gamma(B\to V(\to P_1P_2)\ell^+\nu_\ell)}{dq^2 d(\cos\theta^*)} = \frac{3}{4}[2F_L(q^2)\cos^2\theta^* + F_T(q^2)\sin^2\theta^*]. \quad (23)$$

TABLE IV. The branching ratios, FB asymmetry and polarization parameters of semileptonic B decays in RQM.

Decay	Br	$\langle A_{\rm FB}\rangle$	$\langle C_F^\ell\rangle$	$\langle P_L^\ell\rangle$	$\langle P_T^\ell\rangle$	$\langle F_L\rangle$
$B^+\to\bar D^0 e^+\nu_e$	2.53×10^{-2}	-0.98×10^{-6}	−1.50	1.00	-1.01×10^{-3}	
$B^+\to\bar D^0\mu^+\nu_\mu$	2.52×10^{-2}	−0.013	−1.46	0.96	−0.19	
$B^+\to\bar D^0\tau^+\nu_\tau$	0.68×10^{-2}	−0.37	−0.30	−0.24	−0.85	
$B^+\to\bar D^{*0} e^+\nu_e$	6.81×10^{-2}	−0.22	−0.48	1.00	-0.34×10^{-3}	0.55
$B^+\to\bar D^{*0}\mu^+\nu_\mu$	6.77×10^{-2}	−0.23	−0.47	0.98	−0.061	0.55
$B^+\to\bar D^{*0}\tau^+\nu_\tau$	1.56×10^{-2}	−0.32	−0.060	0.48	−0.12	0.47
$B^+\to\pi^0 e^+\nu_e$	7.20×10^{-5}	-0.28×10^{-6}	−1.50	1.00	-0.46×10^{-3}	
$B^+\to\pi^0\mu^+\nu_\mu$	0.72×10^{-4}	−0.004	−1.49	0.99	−0.09	
$B^+\to\pi^0\tau^+\nu_\tau$	0.45×10^{-4}	−0.22	−0.82	0.42	−0.72	
$B^+\to\rho e^+\nu_e$	1.74×10^{-4}	−0.50	0.042	1.00	-0.07×10^{-3}	0.31
$B^+\to\rho^0\mu^+\nu_\mu$	1.73×10^{-4}	−0.51	0.047	0.99	−0.011	0.31
$B^+\to\rho^0\tau^+\nu_\tau$	0.97×10^{-4}	−0.54	0.14	0.60	0.095	0.31
$B^+\to\eta e^+\nu_e$	4.24×10^{-5}	-0.37×10^{-6}	−1.50	1.00	-0.60×10^{-3}	
$B^+\to\eta\mu^+\nu_\mu$	0.42×10^{-4}	−0.006	−1.48	0.98	−0.12	
$B^+\to\eta\tau^+\nu_\tau$	0.26×10^{-4}	−0.27	−0.67	0.21	−0.83	
$B^+\to\eta' e^+\nu_e$	3.17×10^{-5}	-0.43×10^{-6}	−1.50	1.00	-0.66×10^{-3}	
$B^+\to\eta'\mu^+\nu_\mu$	0.31×10^{-4}	−0.007	−1.48	0.98	−0.13	
$B^+\to\eta'\tau^+\nu_\tau$	0.17×10^{-4}	−0.30	−0.59	0.14	−0.84	
$B^+\to\omega e^+\nu_e$	1.71×10^{-4}	−0.43	−0.17	1.00	-0.12×10^{-3}	0.41
$B^+\to\omega\mu^+\nu_\mu$	1.71×10^{-4}	−0.43	−0.16	0.99	−0.02	0.41
$B^+\to\omega\tau^+\nu_\tau$	0.97×10^{-4}	−0.49	0.009	0.59	−0.007	0.40

Here the longitudinal polarization fraction of the final vector meson has the following form in terms of the helicity structures [11,21]:

$$F_L(q^2) = \frac{\mathcal{H}_L(1+\frac{m_\ell^2}{2q^2}) + \frac{3m_\ell^2}{2q^2}\mathcal{H}_S}{\mathcal{H}_{\rm total}}, \tag{24}$$

and its transverse polarization fraction $F_T(q^2) = 1 - F_L(q^2)$.

For $\bar{B} \to F\ell^-\bar{\nu}_\ell$ decays the charge of the lepton is negative, and thus expressions for the FB asymmetry, leptonic longitudinal and transverse polarization change due to the different sign in the leptonic tensor. They are the following

$$A_{\rm FB}(q^2) = -\frac{3}{4}\frac{\mathcal{H}_P + 2\frac{m_\ell^2}{q^2}\mathcal{H}_{SL}}{\mathcal{H}_{\rm total}}, \tag{25}$$

$$P_L^\ell(q^2) = -\frac{(\mathcal{H}_U + \mathcal{H}_L)(1-\frac{m_\ell^2}{2q^2}) - \frac{3m_\ell^2}{2q^2}\mathcal{H}_S}{\mathcal{H}_{\rm total}}, \tag{26}$$

$$P_T^\ell(q^2) = -\frac{3\pi m_\ell}{8\sqrt{q^2}}\frac{\mathcal{H}_P - 2\mathcal{H}_{SL}}{\mathcal{H}_{\rm total}}. \tag{27}$$

The expressions for $C_F^\ell(q^2)$ and $F_{L(T)}(q^2)$ do not change.

The mean values of the FB asymmetry $\langle A_{\rm FB}\rangle$ and polarization $\langle C_F^\ell\rangle$, $\langle P_{L,T}^\ell\rangle$, $\langle F_L\rangle$ parameters are calculated

TABLE V. The branching ratios, FB asymmetry and polarization parameters of semileptonic B_s decays in RQM.

Decay	Br	$\langle A_{\rm FB}\rangle$	$\langle C_F^\ell\rangle$	$\langle P_L^\ell\rangle$	$\langle P_T^\ell\rangle$	$\langle F_L\rangle$
$B_s \to D_s^- e^+\nu_e$	2.12×10^{-2}	-0.97×10^{-6}	-1.50	1.00	-1.02×10^{-3}	
$B_s \to D_s^-\mu^+\nu_\mu$	2.12×10^{-2}	-0.013	-1.46	0.96	-0.19	
$B_s \to D_s^-\tau^+\nu_\tau$	0.61×10^{-2}	-0.36	-0.30	-0.27	-0.85	
$B_s \to D_s^{*-} e^+\nu_e$	5.06×10^{-2}	-0.26	-0.35	1.00	-0.23×10^{-3}	0.49
$B_s \to D_s^{*-}\mu^+\nu_\mu$	5.05×10^{-2}	-0.27	-0.33	0.99	-0.040	0.49
$B_s \to D_s^{*-}\tau^+\nu_\tau$	1.23×10^{-2}	-0.32	-0.040	0.53	-0.035	0.42
$B_s \to K^- e^+\nu_e$	15.6×10^{-5}	-0.39×10^{-6}	-1.50	1.00	-0.56×10^{-3}	
$B_s \to K^-\mu^+\nu_\mu$	1.55×10^{-4}	-0.006	-1.48	0.98	-0.11	
$B_s \to K^-\tau^+\nu_\tau$	0.91×10^{-4}	-0.24	-0.77	0.35	-0.75	
$B_s \to K^{*-} e^+\nu_e$	3.29×10^{-4}	-0.37	-0.23	1.00	-0.14×10^{-3}	0.44
$B_s \to K^{*-}\mu^+\nu_\mu$	3.29×10^{-4}	-0.38	-0.22	0.99	-0.025	0.44
$B_s \to K^{*-}\tau^+\nu_\tau$	1.82×10^{-4}	-0.44	-0.032	0.63	-0.025	0.42

TABLE VI. The branching ratios, FB asymmetry and polarization parameters of semileptonic B_c decays in RQM.

Decay	Br	$\langle A_{\rm FB}\rangle$	$\langle C_F^\ell\rangle$	$\langle P_L^\ell\rangle$	$\langle P_T^\ell\rangle$	$\langle F_L\rangle$
$B_c^+ \to \eta_c e^+\nu_e$	0.42×10^{-2}	-8.6×10^{-7}	-1.5	1.0	-1.03×10^{-3}	
$B_c^+ \to \eta_c\mu^+\nu_\mu$	0.42×10^{-2}	-0.012	-1.46	0.96	-0.20	
$B_c^+ \to \eta_c\tau^+\nu_\tau$	0.16×10^{-2}	-0.35	-0.24	-0.39	-0.82	
$B_c^+ \to J/\psi e^+\nu_e$	1.31×10^{-2}	-0.19	-0.23	1.0	-0.15×10^{-3}	0.44
$B_c^+ \to J/\psi\mu^+\nu_\mu$	1.30×10^{-2}	-0.19	-0.23	0.99	-0.028	0.44
$B_c^+ \to J/\psi\tau^+\nu_\tau$	0.37×10^{-2}	-0.23	-0.032	0.56	-0.069	0.40
$B_c^+ \to \bar{D}^0 e^+\nu_e$	0.33×10^{-4}	-1.0×10^{-7}	-1.5	1.0	-0.43×10^{-3}	
$B_c^+ \to \bar{D}^0\mu^+\nu_\mu$	0.33×10^{-4}	-0.002	-1.49	0.99	-0.088	
$B_c^+ \to \bar{D}^0\tau^+\nu_\tau$	0.28×10^{-4}	-0.257	-0.72	0.25	-0.83	
$B_c^+ \to \bar{D}^{*0} e^+\nu_e$	0.84×10^{-4}	-0.45	0.10	1.0	6.7×10^{-5}	0.29
$B_c^+ \to \bar{D}^{*0}\mu^+\nu_\mu$	0.84×10^{-4}	-0.45	0.10	1.0	0.014	0.29
$B_c^+ \to \bar{D}^{*0}\tau^+\nu_\tau$	0.55×10^{-4}	-0.42	0.072	0.78	0.22	0.29
$B_c^+ \to B_s e^+\nu_e$	0.92×10^{-2}	-1.1×10^{-5}	-1.5	1	-0.004	
$B_c^+ \to B_s\mu^+\nu_\mu$	0.90×10^{-2}	-0.093	-1.21	0.73	-0.57	
$B_c^+ \to B_s^* e^+\nu_e$	2.30×10^{-2}	-0.15	-0.29	1	-7.3×10^{-4}	0.46
$B_c^+ \to B_s^*\mu^+\nu_\mu$	2.20×10^{-2}	-0.17	-0.23	0.93	-0.09	0.46
$B_c^+ \to B e^+\nu_e$	4.94×10^{-4}	-9.0×10^{-6}	-1.5	1	-0.004	
$B_c^+ \to B\mu^+\nu_\mu$	4.79×10^{-4}	-0.080	-1.25	0.76	-0.53	
$B_c^+ \to B^* e^+\nu_e$	17.9×10^{-4}	-0.17	-0.27	1	-6.2×10^{-4}	0.45
$B_c^+ \to B^*\mu^+\nu_\mu$	17.2×10^{-4}	-0.18	-0.22	0.94	-0.09	0.45

by separately integrating their corresponding numerators and denominators with inclusion of the common kinematical factor $\lambda^{1/2}q^2(1-m_\ell^2/q^2)^2$.

We give predictions for the branching fractions, FB asymmetry and polarization parameters of semileptonic B, B_s, and B_c meson decays calculated with the form factors of RQM in Tables IV–VI. The branching fractions are calculated using the following values of CKM matrix elements: $|V_{cb}| = 0.039$, $|V_{ub}| = 0.0040$, $|V_{cs}| = 0.987$, $|V_{cd}| = 0.221$. All meson and lepton masses are taken from PDG [1]. We roughly estimate the uncertainties of our predictions for the branching fraction values given in Tables IV–VI, which arise from the model to be about 10%, and if we also include uncertainties of the CKM matrix elements the estimate of the total uncertainty is about 15%.

V. COMPARISON OF RQM AND CLFQM PREDICTIONS

In this section we compare predictions for semileptonic decay form factors, decay rates and FB asymmetries in RQM and the other popular quark model CLFQM [10] and confront them with available experimental data and lattice calculations. The form factors of semileptonic B meson decays in CLFQM are given in Refs. [10,11]. In the following tables, the results in CLFQM are mainly from Ref. [11].

In Table VII we present predictions for the form factors of the weak B and B_s meson transitions at $q^2 = 0$ and $q^2 = q^2_{\rm max}$ in RQM and CLFQM. We find that the form factor values at $q^2 = 0$ are close in both models for all considered decays. The values of form factors at $q^2 = q^2_{\rm max}$ are also close for B and B_s decays to heavy $D^{(*)}$ and $D_s^{(*)}$ mesons. They are consistent with the recent lattice QCD calculations [22–26]. On the other hand, the values of form factors for heavy-to-light transitions at $q^2 = q^2_{\rm max}$ significantly differ in the considered models. The values of form factors at this kinematic point in RQM are substantially higher than the ones in CLFQM.

In Fig. 1 we plot the form factors $f_+(q^2)$ and $f_0(q^2)$ of the $B \to \pi$ semileptonic transitions in the whole kinematic range. Predictions of RQM are plotted by solid blue lines and those of CLFQM are given by dashed orange lines. From this plot we see that the form factor $f_+(q^2)$ in RQM rapidly grows for $q^2 > 15$ GeV^2 up to the value $f_+(q^2_{\rm max}) = 10.9$, while this form factor in CLFQM reaches only the value $f_+(q^2_{\rm max}) = 1.27$ which is almost an order of magnitude lower. In the same figure we also give lattice QCD results [27–32] which are available in the high $q^2 > 15$ GeV^2 region. The form factors of the $B_s \to K$ semileptonic transitions in RQM and CLFQM in comparison with lattice QCD data [30,32–34] are plotted in Fig. 2. The model predictions are again significantly different for the form factor $f_+(q^2)$. It rapidly grows in RQM, contrary in CLFQM it slowly increases reaching the maximum value at q^2 of about 15 GeV^2 and then slowly decreases. Note that in CLFQM the value of $f_+(q^2_{\rm max})$ is even smaller than the value of $f_0(q^2_{\rm max})$. From these plots we see that predictions of RQM for the form factor f_+ are in much better agreement with lattice data, which also favor its rapid growth with q^2.

The main reason for the discrepancy between the q^2 dependence of the heavy-to-light form factors in Figs. 1 and 2 in RQM and CLFQM is the following. In RQM the form factors are directly calculated in the whole $0 \le q^2 \le q^2_{\rm max}$ region without any extrapolations. As the result the pole structure of the form factors $f_+(q^2)$, $V(q^2)$ and $A_0(q^2)$ in

TABLE VII. Comparison of form factors of the weak B and B_s meson transitions in RQM and CLFQM.

		$F(0)$		$F(q^2_{\rm max})$	
Transition	Form factor	RQM	CLFQM	RQM	CLFQM
$B \to D$	f_+	0.696	0.67	1.24	1.21
	f_0	0.696	0.67	0.82	0.91
$B \to D^*$	V	0.915	0.77	1.38	1.34
	A_0	0.814	0.68	1.21	1.15
	A_1	0.730	0.65	0.83	0.84
	A_2	0.627	0.62	1.02	0.99
$B \to \pi$	f_+	0.217	0.25	10.9	1.27
	f_0	0.217	0.25	1.32	0.82
$B \to \rho$	V	0.295	0.29	2.80	1.06
	A_0	0.231	0.32	2.19	1.00
	A_1	0.269	0.24	0.439	0.53
	A_2	0.282	0.22	1.92	0.70
$B \to \eta$	f_+	0.194	0.22	2.75	1.31
	f_0	0.194	0.22	0.52	0.52
$B \to \eta'$	f_+	0.187	0.18	1.34	0.75
	f_0	0.187	0.18	0.32	0.35
$B \to \omega$	V	0.263	0.27	2.47	0.88
	A_0	0.244	0.28	1.96	0.60
	A_1	0.232	0.23	0.46	0.53
	A_2	0.229	0.21	0.96	0.63
$B_s \to D_s$	f_+	0.663	0.67	1.23	1.20
	f_0	0.663	0.67	0.87	0.92
$B_s \to D_s^*$	V	0.925	0.75	1.48	1.30
	A_0	0.625	0.66	1.03	1.13
	A_1	0.668	0.62	0.82	0.84
	A_2	0.723	0.57	1.09	0.94
$B_s \to K$	f_+	0.284	0.23	5.42	0.42
	f_0	0.284	0.23	0.459	0.64
$B_s \to K^*$	V	0.291	0.23	3.06	0.32
	A_0	0.289	0.25	2.10	0.34
	A_1	0.287	0.19	0.581	0.36
	A_2	0.286	0.16	0.953	0.25

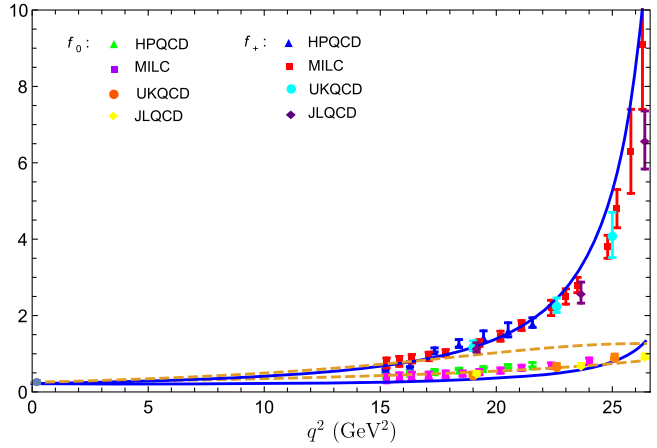

FIG. 1. Comparison of theoretical predictions for the form factors of the weak $B \to \pi$ transitions. Model results: the RQM form factors are given by solid blue lines, and the CLFQM form factors are plotted by orange dashed lines. Upper curves correspond to $f_+(q^2)$ and the lower ones to $f_0(q^2)$. Lattice results are plotted: HPQCD [27] by triangles [blue $f_+(q^2)$, green $f_0(q^2)$] with error bars, FNAL/MILC [28,29] by squares [red $f_+(q^2)$, magenta $f_0(q^2)$] with error bars, RBC/UKQCD [30] by filled circles [cyan $f_+(q^2)$, orange $f_0(q^2)$] with error bars, and JLQCD [31] by diamonds [purple $f_+(q^2)$, yellow $f_0(q^2)$].

Eq. (10) is explicitly obtained already in the impulse approximation. The inclusion of the negative-energy contributions (Z-diagrams) enhances the growth of these form factors for the heavy-to-light decays in the high q^2 region, bringing results in a better agreement with lattice data. Contrary, in CLFQM the $q^+ = 0$ frame (light-cone gauge) is used, resulting in the determination of the form factors for $q^2 < 0$, and then they are extrapolated to the $q^2 > 0$ region. As has been shown in Refs. [35,36], for the $q^+ = 0$ case, the nonvalence contributions (Z- diagrams) are highly suppressed, leading to a relativistic picture of a meson as only the valence $q\bar{q}$ structure. Such extrapolation works well for the heavy-to-heavy transitions with a rather small q^2 range, but fails to reproduce the pole structure of the form factors $f_+(q^2)$, $V(q^2)$ and $A_0(q^2)$ for the heavy-to-light transitions which have a very broad q^2 range. One

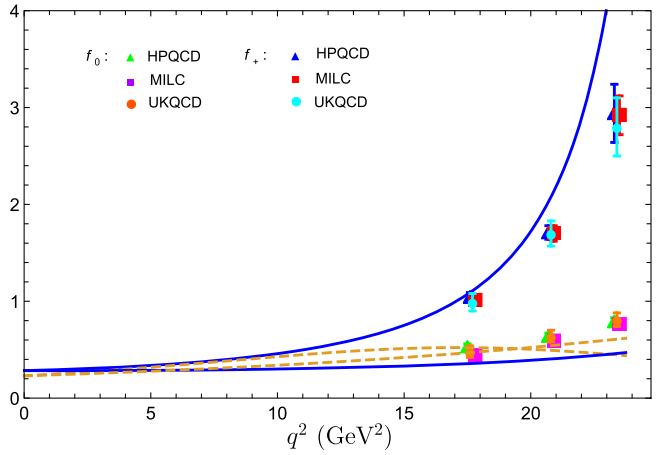

FIG. 2. Same as in Fig. 1, but for the form factors of the weak $B_s \to K$ transitions. For the orange dashed lines, the upper one below $q^2 < 15$ GeV^2 corresponds to $f_+(q^2)$, and the lower one $f_0(q^2)$. HPQCD, MILC and UKQCD data are from Refs. [27,30,34], respectively.

TABLE VIII. Comparison of theoretical predictions for the semileptonic decay branching ratios with available experimental data [1].

	Theory		
Decay	RQM	CLFQM	Experiment
$B^+ \to \bar{D}^0 \ell^+ \nu_\ell$	2.52%	2.22%	$(2.35 \pm 0.09)\%$
$B^+ \to \bar{D}^0 \tau^+ \nu_\tau$	6.8×10^{-3}	6.7×10^{-3}	$(7.7 \pm 2.5) \times 10^{-3}$
$B^+ \to \bar{D}^{*0} \ell^+ \nu_\ell$	6.77%	5.70%	$(5.66 \pm 0.22)\%$
$B^+ \to \bar{D}^{*0} \tau^+ \nu_\tau$	1.56%	1.40%	$(1.88 \pm 0.20)\%$
$B^+ \to \pi^0 \ell^+ \nu_\ell$	7.2×10^{-5}	7.8×10^{-5}	$(7.80 \pm 0.27) \times 10^{-5}$
$B^+ \to \eta \ell^+ \nu_\ell$	4.2×10^{-5}	5.4×10^{-5}	$(3.9 \pm 0.5) \times 10^{-5}$
$B^+ \to \eta' \ell^+ \nu_\ell$	3.1×10^{-5}	2.6×10^{-5}	$(2.3 \pm 0.8) \times 10^{-5}$
$B^+ \to \rho^0 \ell^+ \nu_\ell$	1.73×10^{-4}	2.19×10^{-4}	$(1.58 \pm 0.11) \times 10^{-4}$
$B^+ \to \omega \ell^+ \nu_\ell$	1.71×10^{-4}	2.07×10^{-4}	$(1.19 \pm 0.09) \times 10^{-5}$
$B^0 \to D^- \ell^+ \nu_\ell$	2.33%	2.05%	$(2.31 \pm 0.10)\%$
$B^0 \to D^- \tau^+ \nu_\tau$	0.63%	0.62%	$(1.08 \pm 0.23)\%$
$B^0 \to D^{*-} \ell^+ \nu_\ell$	6.28%	5.28%	$(5.06 \pm 0.12)\%$
$B^0 \to D^{*-} \tau^+ \nu_\tau$	1.45%	1.30%	$(1.57 \pm 0.09)\%$
$B^0 \to \pi^- \ell^+ \nu_\ell$	1.33×10^{-4}	1.44×10^{-4}	$(1.50 \pm 0.06) \times 10^{-4}$
$B^0 \to \pi^- \tau^+ \nu_\tau$	0.84×10^{-4}	0.98×10^{-4}	$< 2.5 \times 10^{-4}$
$B^0 \to \rho^- \ell^+ \nu_\ell$	3.2×10^{-4}	4.1×10^{-4}	$(2.94 \pm 0.21) \times 10^{-4}$
$B_s \to D_s^- \mu^+ \nu_\mu$	2.12%	2.05%	$(2.52 \pm 0.24)\%$
$B_s \to D_s^{*-} \mu^+ \nu_\mu$	5.05%	5.05%	$(5.4 \pm 0.5)\%$
$B_s \to K^- \mu^+ \nu_\mu$	1.55×10^{-4}	1.01×10^{-4}	$(1.06 \pm 0.10) \times 10^{-4}$

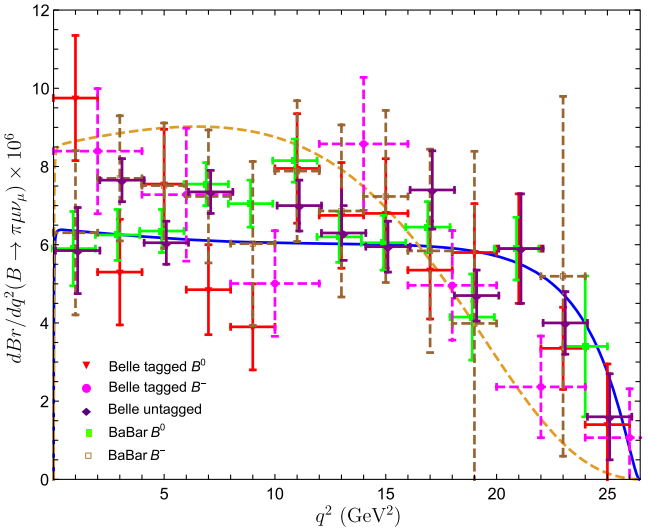

FIG. 3. Differential branching fractions of the semileptonic $B \to \pi\mu\nu_\mu$ decay. Comparison of theoretical predictions (RQM—solid blue line, CLFQM—orange dashed line) with available experimental data [37–39].

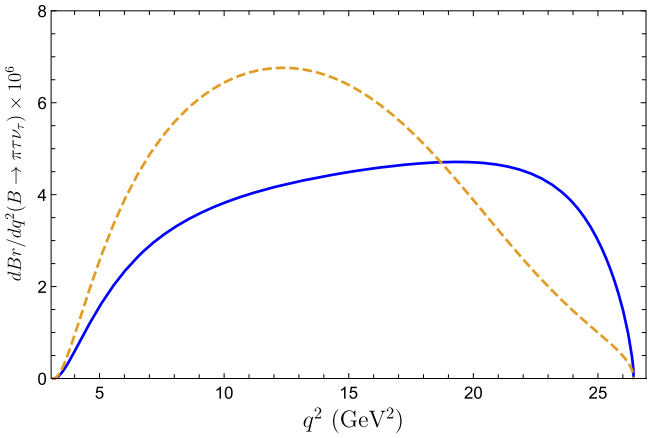

FIG. 4. Differential branching fractions of the semileptonic $B \to \pi\tau\nu_\tau$ decay. Comparison of theoretical predictions (RQM—solid blue lines, CLFQM—orange dashed lines).

may indeed work in the $q^+ \neq 0$ frame, as a more realistic case for the timelike region, then Z- diagrams will be inevitable, and moreover for a larger q^2 region the contribution of Z- diagrams becomes more important. This should be the main origin for the inconsistency between RQM and CLFQM for the heavy-to-light decays, for which we used the $B \to \pi$ and $B_s \to K$ transitions as examples.

In Table VIII we present the comparison of the RQM and CLFQM model predictions for the semileptonic B and B_s decay branching ratios with available experimental data [1]. We see that the branching ratios, which are integrated quantities, are consistent with each other and experimental data. However, the differential distributions can differ substantially due to the difference in the q^2 dependence of the form factors. As an example, in Figs. 3 and 4 we plot the differential branching fractions in both models for $B \to \pi\mu\nu_\mu$ and $B \to \pi\tau\nu_\tau$ decays, respectively. From these plots we see that differential distributions, which are plotted by solid blue line for RQM and orange dashed lines for CLFQM, differ significantly. In Fig. 3 we also show the available experimental data from Belle [37,38] and *BABAR* [39] Collaborations. It is not possible to unambiguously distinguish between models since the data have large uncertainties, but the shape of the differential distribution predicted by RQM is in better agreement with the averaged data.

In Table IX we give the ratios of the decay rates with τ and μ leptons, $\mathcal{R}(F) = \Gamma(B \to F\tau\nu_\tau)/\Gamma(B \to F\mu\nu_\mu)$, predicted by RQM, CLFQM and lattice in comparison with available experimental data. Such comparison provides the test of the lepton universality and deviations of the standard model predictions from experimental data can indicate the possible contributions of new physics. We see that theoretical predictions are consistent with each other and are lower than experimental data by about $1 \sim 3\sigma$.

For the semileptonic $\bar{B} \to D^*\tau^-\bar{\nu}_\tau$ decay the τ-lepton polarization and longitudinal polarization fraction of the final vector D^* meson were recently measured experimentally [41,42]. We compare RQM, CLFQM and lattice predictions with these data in Table X. The theoretical

TABLE IX. Ratios of the decay rates with τ and μ leptons $\mathcal{R}(F) = \Gamma(B \to F\tau\nu_\tau)/\Gamma(B \to F\mu\nu_\mu)$ in comparison with available lattice or experimental data, cf. Ref. [3] and references therein.

	Theory			Experiment		
Transition	RQM	CLFQM	Lattice/SM analysis [3]	PDG [1]	HFLAV [40]	[3]
$B \to D$	0.271	0.302	0.298(3)	0.429(82)(52)(B^+) 0.469(84)(53)(B^0)	0.339(26)(14)	0.337(30)
$B \to D^*$	0.231	0.246	0.250(3)	0.335(34)(B^+) 0.309(16)(B^0)	0.295(10)(10)	0.298(14)
$B \to \pi$	0.631	0.680	0.641(16)			1.05(51)
$B \to \rho$	0.561	0.543	0.535(8)			
$B \to \eta$	0.629	0.611				
$B \to \eta'$	0.544	0.538				
$B \to \omega$	0.566	0.531	0.546(15)			
$B_s \to D_s$	0.287	0.298	0.297(3)			
$B_s \to D_s^*$	0.244	0.248	0.247(8)			
$B_s \to K$	0.588	0.673				
$B_s \to K^*$	0.553	0.520				
$B_c \to \eta_c$	0.373					
$B_c \to J/\psi$	0.284		0.2582(38)	0.71(17)(18)		
$B_c \to D$	0.833					
$B_c \to D^*$	0.656					

TABLE X. Comparison of theoretical predictions for the τ-lepton polarization and longitudinal polarization fraction of the final vector meson with experimental data [41,42].

	$\langle P_L^\tau \rangle$				$\langle F_L \rangle$			
Decay	RQM	CLFQM	Lattice [32]	Experiment	RQM	CLFQM	Lattice [32]	Experiment
$\bar{B} \to D^* \tau^- \bar{\nu}_\tau$	−0.48	−0.51	−0.529(7)	$-0.38(51)(^{21}_{10})$	0.47	0.45	0.414(12)	0.60(8)(4)
$\bar{B}_s \to D_s^* \tau^- \bar{\nu}_\tau$	−0.53	−0.51	−0.520(12)		0.42	0.45	0.404(16)	

TABLE XI. Comparison of RQM and CLFQM predictions with lattice data for FB asymmetry and lepton polarization for B decays to light pseudoscalar mesons.

	$\langle A_{\rm FB} \rangle$			$\langle P_L^\ell \rangle$		
Decay	RQM	CLFQM	Lattice [32]	RQM	CLFQM	Lattice [32]
$B \to \pi \mu^+ \nu_\mu$	−0.004	−0.005	−0.0034(31)	0.99	0.98	0.988(9)
$\bar{B} \to \pi \tau^+ \nu_\tau$	−0.22	−0.28	−0.220(24)	0.42	0.087	0.301(86)
$\bar{B}_s \to K \mu^+ \nu_\mu$	−0.006	−0.007	−0.0046(28)	0.98	0.98	0.986(7)
$\bar{B}_s \to K \tau^+ \nu_\tau$	−0.24	−0.29	−0.262(23)	0.35	−0.10	0.172(91)

predictions for the τ-lepton longitudinal polarization $\langle P_L^\tau \rangle$ agree with each other and experimental data within large error bars. The experimental value for the longitudinal polarization fraction of the final vector D^* meson $\langle F_L \rangle$ is about 2σ higher than theoretical predictions.

In Table XI we compare RQM and CLFQM predictions with lattice data for the FB asymmetry and lepton polarization for the heavy-to-light semileptonic B and B_s decays to light pseudoscalar mesons. Such comparison is important since RQM and CLFQM have significantly different

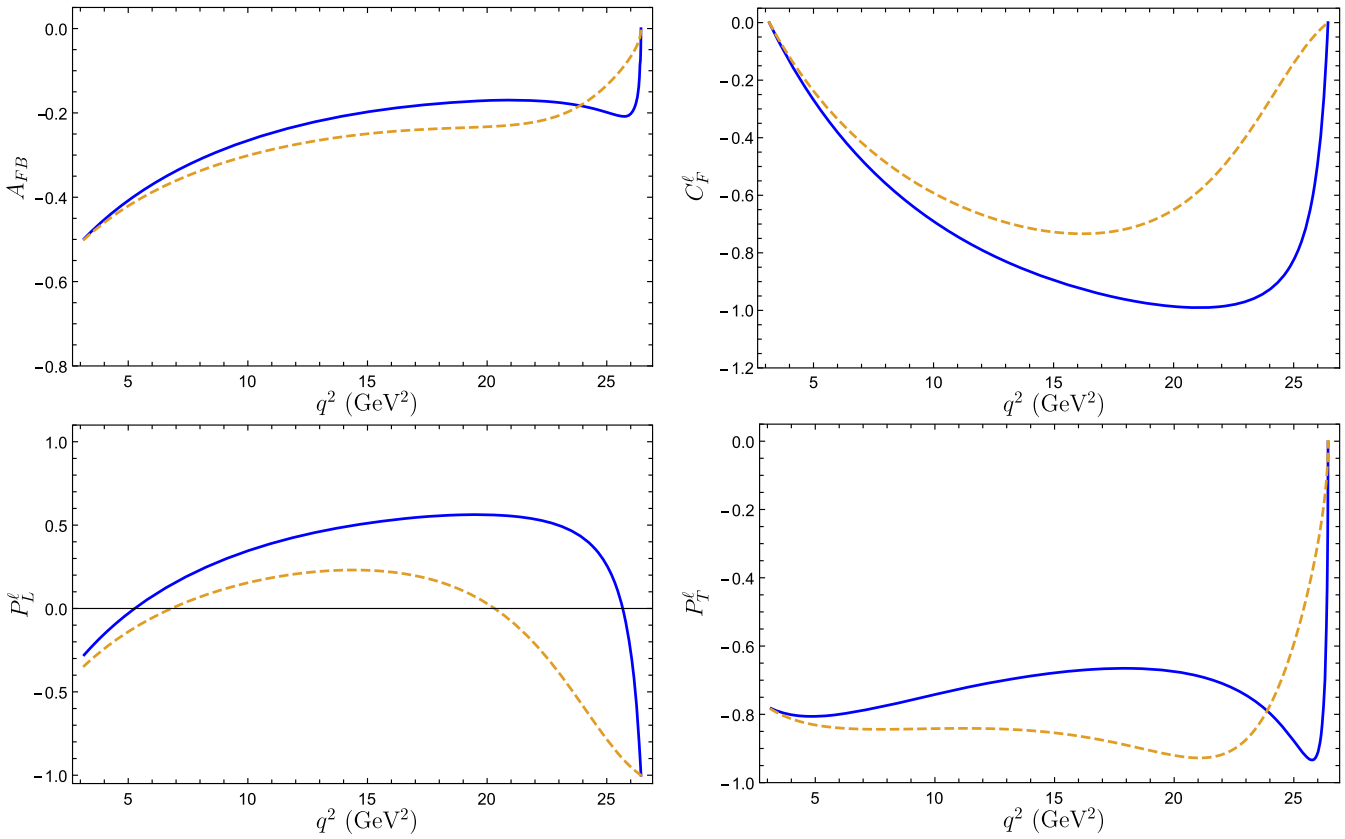

FIG. 5. Comparison of theoretical predictions for the differential FB asymmetry $A_{\rm FB}$ and polarization C_F^ℓ, $P_{L,T}^\ell$ parameters for the semileptonic $B \to \pi \tau^+ \nu_\tau$ decay. RQM result are given by blue solid lines and CLFQM results are given by orange dashed lines.

TABLE XII. The branching ratios, FB asymmetry, and polarization parameters of the semileptonic B decays. For each channel, the result for RQM is shown in the upper line and the one for CLFQM in the lower line.

Decay	Br	$\langle A_{\rm FB}\rangle$	$\langle C_F^\ell\rangle$	$\langle P_L^\ell\rangle$	$\langle P_T^\ell\rangle$	$\langle F_L\rangle$
$B^+ \to \bar{D}^0 e^+ \nu_e$	2.53×10^{-2}	-0.98×10^{-6}	-1.50	1.00	-1.01×10^{-3}	
	2.23×10^{-2}	-1.04×10^{-6}	-1.50	1.00	-1.07×10^{-3}	
$B^+ \to \bar{D}^0 \mu^+ \nu_\mu$	2.52×10^{-2}	-0.013	-1.46	0.96	-0.19	
	2.22×10^{-2}	-0.014	-1.46	0.96	-0.20	
$B^+ \to \bar{D}^0 \tau^+ \nu_\tau$	0.68×10^{-2}	-0.37	-0.30	-0.24	-0.85	
	0.67×10^{-2}	-0.36	-0.27	-0.32	-0.84	
$B^+ \to \bar{D}^{*0} e^+ \nu_e$	6.81×10^{-2}	-0.22	-0.48	1.00	-0.34×10^{-3}	0.55
	5.43×10^{-2}	-0.22	-0.42	1.00	-0.29×10^{-3}	0.52
$B^+ \to \bar{D}^{*0} \mu^+ \nu_\mu$	6.77×10^{-2}	-0.23	-0.47	0.98	-0.061	0.55
	5.70×10^{-2}	-0.23	-0.41	0.98	-0.052	0.52
$B^+ \to \bar{D}^{*0} \tau^+ \nu_\tau$	1.56×10^{-2}	-0.32	-0.060	0.48	-0.12	0.47
	1.40×10^{-2}	-0.30	-0.056	0.51	-0.10	0.45
$B^+ \to \pi^0 e^+ \nu_e$	7.20×10^{-5}	-0.28×10^{-6}	-1.50	1.00	-0.46×10^{-3}	
	7.89×10^{-5}	-0.35×10^{-6}	-1.50	1.00	-0.62×10^{-3}	
$B^+ \to \pi^0 \mu^+ \nu_\mu$	0.72×10^{-4}	-0.004	-1.49	0.99	-0.09	
	0.78×10^{-4}	-0.005	-1.48	0.98	-0.12	
$B^+ \to \pi^0 \tau^+ \nu_\tau$	4.5×10^{-5}	-0.22	-0.82	0.42	-0.72	
	5.3×10^{-5}	-0.28	-0.59	0.087	-0.85	
$B^+ \to \rho^0 e^+ \nu_e$	1.74×10^{-4}	-0.50	0.042	1.00	-0.07×10^{-3}	0.31
	2.19×10^{-4}	-0.32	-0.39	1.00	-0.18×10^{-3}	0.51
$B^+ \to \rho^0 \mu^+ \nu_\mu$	1.73×10^{-4}	-0.51	0.047	0.99	-0.011	0.31
	2.19×10^{-4}	-0.32	-0.39	0.99	-0.03	0.51
$B^+ \to \rho^0 \tau^+ \nu_\tau$	0.97×10^{-4}	-0.54	0.14	0.60	0.095	0.31
	1.19×10^{-4}	-0.39	-0.12	0.60	-0.10	0.49
$B^+ \to \eta e^+ \nu_e$	4.24×10^{-5}	-0.37×10^{-6}	-1.50	1.00	-0.60×10^{-3}	
	5.44×10^{-5}	-0.39×10^{-6}	-1.50	1.00	-0.64×10^{-3}	
$B^+ \to \eta \mu^+ \nu_\mu$	0.42×10^{-4}	-0.006	-1.48	0.98	-0.12	
	0.54×10^{-4}	-0.006	-1.48	0.98	-0.12	
$B^+ \to \eta \tau^+ \nu_\tau$	2.6×10^{-5}	-0.27	-0.67	0.21	-0.83	
	3.3×10^{-5}	-0.29	-0.60	0.11	-0.86	
$B^+ \to \eta' e^+ \nu_e$	3.17×10^{-5}	-0.43×10^{-6}	-1.50	1.00	-0.66×10^{-3}	
	2.64×10^{-5}	-0.49×10^{-6}	-1.50	1.00	-0.72×10^{-3}	
$B^+ \to \eta' \mu^+ \nu_\mu$	0.31×10^{-4}	-0.007	-1.48	0.98	-0.13	
	0.26×10^{-4}	-0.007	-1.47	0.98	-0.14	
$B^+ \to \eta' \tau^+ \nu_\tau$	1.7×10^{-5}	-0.30	-0.59	0.14	-0.84	
	1.4×10^{-5}	-0.31	-0.52	0.026	-0.87	
$B^+ \to \omega e^+ \nu_e$	1.71×10^{-4}	-0.43	-0.17	1.00	-0.12×10^{-3}	0.41
	2.08×10^{-4}	-0.30	-0.42	1.00	-0.15×10^{-3}	0.51
$B^+ \to \omega \mu^+ \nu_\mu$	1.71×10^{-4}	-0.43	-0.16	0.99	-0.02	0.41
	2.07×10^{-4}	-0.30	-0.41	0.99	-0.027	0.52
$B^+ \to \omega \tau^+ \nu_\tau$	0.97×10^{-4}	-0.49	0.009	0.59	-0.007	0.40
	1.10×10^{-4}	-0.36	-0.15	0.65	-0.06	0.49

dependence of the form factor $f_+(q^2)$ for large values of q^2. From this table we see that the lepton polarization $\langle P_L^\tau \rangle$ is very sensitive to the employed model. Its values are substantially smaller in CLFQM, and for $B_s \to K\tau^+\nu_\tau$ they have even opposite signs. In general RQM results for these observables agree better with the combined lattice values.

In Fig. 5 we, as an example, present comparison of RQM and CLFQM predictions for the quantities $A_{\rm FB}(q^2)$, $C_F^\ell(q^2)$, $P_{L,T}^\ell(q^2)$ for the semileptonic $B \to \pi\tau^+\nu_\tau$ decay. The RQM results are plotted by the blue solid lines and CLFQM ones by orange dashed line. The q^2 dependence of these FB asymmetry and polarization parameters is determined by the corresponding dependence of the form factors and thus is significantly different.

Finally, we present a detailed comparison of the branching ratios, FB asymmetry and polarization parameters of the semileptonic B and B_s decays in RQM and CLFQM in Tables XII and XIII. The branching fractions are close for all decay modes. The predictions for FB asymmetry and polarization parameters for the heavy-to-heavy ($B \to D^{(*)}\ell\nu_\ell$ and $B_s \to D_s^{(*)}\ell\nu_\ell$) semileptonic decays are also compatible in considered models. This is expected, since the heavy-to-heavy form factors have similar q^2 behavior in both models. The main differences are found in these parameters for the heavy-to-light transitions. Therefore the measurement of those observables can help to discriminate between theoretical models.

(i) For decays to light pseudoscalar mesons, the most sensitive observables are in the τ sector.

As was already noted (see Table XI), it is the longitudinal polarization fraction of τ-lepton $\langle P_L^\tau \rangle$, which values in models differ substantially and even have the opposite signs for the $B_s \to K^-\tau^+\nu_\tau$ decay; the other observable is the FB asymmetry $\langle A_{\rm FB} \rangle$, whose values are higher in CLFQM. On the other hand, the absolute values of $\langle C_F^\tau \rangle$ are systematically higher in RQM and for the $B_s \to K^-\tau^+\nu_\tau$ decay its value in RQM is about 1.7 times larger than the one in CLFQM.

TABLE XIII. The branching ratios, FB asymmetry and polarization parameters of the semileptonic B_s decays. For each channel, the result for RQM is shown in the upper line and the one for CLFQM in the lower line.

Decay	Br	$\langle A_{\rm FB} \rangle$	$\langle C_F^\ell \rangle$	$\langle P_L^\ell \rangle$	$\langle P_T^\ell \rangle$	$\langle F_L \rangle$
$B_s \to D_s^- e^+\nu_e$	2.12×10^{-2}	-0.97×10^{-6}	-1.50	1.00	-1.02×10^{-3}	
	2.06×10^{-2}	-1.05×10^{-6}	-1.50	1.00	-1.07×10^{-3}	
$B_s \to D_s^- \mu^+\nu_\mu$	2.12×10^{-2}	-0.013	-1.46	0.96	-0.19	
	2.05×10^{-2}	-0.014	-1.46	0.96	-0.20	
$B_s \to D_s^- \tau^+\nu_\tau$	0.61×10^{-2}	-0.36	-0.30	-0.27	-0.85	
	0.61×10^{-2}	-0.36	-0.26	-0.33	-0.84	
$B_s \to D_s^{*-} e^+\nu_e$	5.06×10^{-2}	-0.26	-0.35	1.00	-0.23×10^{-3}	0.49
	5.07×10^{-2}	-0.22	-0.43	1.00	-0.29×10^{-3}	0.52
$B_s \to D_s^{*-} \mu^+\nu_\mu$	5.05×10^{-2}	-0.27	-0.33	0.99	-0.040	0.49
	5.05×10^{-2}	-0.22	-0.41	0.98	-0.052	0.52
$B_s \to D_s^{*-} \tau^+\nu_\tau$	1.23×10^{-2}	-0.32	-0.040	0.53	-0.035	0.42
	1.25×10^{-2}	-0.29	-0.058	0.51	-0.10	0.45
$B_s \to K^- e^+\nu_e$	15.6×10^{-5}	-0.39×10^{-6}	-1.50	1.00	-0.56×10^{-3}	
	10.1×10^{-5}	-0.43×10^{-6}	-1.50	1.00	-0.72×10^{-3}	
$B_s \to K^- \mu^+\nu_\mu$	1.55×10^{-4}	-0.006	-1.48	0.98	-0.11	
	1.01×10^{-4}	-0.007	-1.48	0.98	-0.14	
$B_s \to K^- \tau^+\nu_\tau$	9.1×10^{-5}	-0.24	-0.77	0.35	-0.75	
	6.8×10^{-5}	-0.29	-0.46	-0.10	-0.86	
$B_s \to K^{*-} e^+\nu_e$	3.29×10^{-4}	-0.37	-0.23	1.00	-0.14×10^{-3}	0.44
	3.30×10^{-4}	-0.21	-0.59	1.00	-0.17×10^{-3}	0.59
$B_s \to K^{*-} \mu^+\nu_\mu$	3.29×10^{-4}	-0.38	-0.22	0.99	-0.025	0.44
	3.29×10^{-4}	-0.21	-0.59	0.99	-0.032	0.59
$B_s \to K^{*-} \tau^+\nu_\tau$	1.82×10^{-4}	-0.44	-0.032	0.63	-0.025	0.42
	1.71×10^{-4}	-0.28	-0.26	0.65	-0.13	0.56

(ii) For decays to light vector mesons:
the main differences are in the lepton-side convexity parameter $\langle C_F^\ell \rangle$ which values differ significantly for all decay modes and for $B^+ \to \rho^0 \ell^+ \nu_\ell$ and $B^+ \to \omega \tau^+ \nu_\tau$ they even have different signs; the values of the FB asymmetry $\langle A_{\rm FB} \rangle$ predicted by RQM are about a factor of 1.5 higher than the ones of CLFQM for all decay modes, while the values of the longitudinal polarization $\langle F_L \rangle$ in RQM are about the same factor smaller than the ones in CLFQM.

VI. CONCLUSIONS

The form factors of the semileptonic B, B_s and B_c decays are calculated in the framework of the relativistic quark model (RQM) based on the quasipotential approach in QCD. These form factors are expressed trough the overlap integrals of the meson wave functions. The wave functions of the initial and final mesons are taken from previous calculations of the meson spectroscopy. All relativistic effects including the wave function transformations from the rest to moving reference frame as well as contributions of the intermediate negative energy states are consistently taken into account. It is important to emphasize that we have not used the heavy quark expansion for description of the heavy-to-heavy meson decays and treated all decays nonperturbatively in the inverse heavy quark mass. Such approach allows us to obtain the values of all form factors in the whole kinematical q^2 range without extrapolations and additional model assumptions. The very accurate and convenient analytic parametrizations, Eqs. (10) and(11), of these form factors were obtained with parameters given in Table I. These form factors can be used for the calculations of various weak decays of bottom mesons.

We use the calculated form factors for the evaluation of the semileptonic branching fractions and differential distributions. In particular we calculate mean values of the forward -backward asymmetry $\langle A_{\rm FB} \rangle$, lepton-side convexity parameter $\langle C_F^\ell \rangle$, longitudinal $\langle P_L^\ell \rangle$ and transverse $\langle P_T^\ell \rangle$ polarization of the charged lepton, and the longitudinal polarization fraction $\langle F_L \rangle$ for the final-state vector meson. These predictions are presented in Tables IV–VI.

Then we compare the results of our calculations with the covariant light-front quark model (CLFQM). The comparison of the form factors shows that both models give consistent values of all form factors at the maximum recoil point of the final meson, $q^2 = 0$. The predicted values of the form factors of the heavy-to-heavy weak transitions at zero recoil point of the final meson, $q^2 = q^2_{\rm max}$, are also compatible. On the other hand, for the heavy-to-light weak transitions, where kinematical range is substantially broader, the values of form factors at $q^2 = q^2_{\rm max}$ differ significantly. The RQM form factors of these transitions grow rapidly with q^2, while CLFQM form factors increase moderately. Such difference in the form factor q^2 dependence results in significantly different differential distributions for bottom meson decays to light mesons. We present a comprehensive comparison of RQM and CLFQM predictions with results of lattice QCD calculations and available experimental data. It was found that the q^2 behavior of the form factor $f_+(q^2)$ for heavy-to-light $B \to \pi$ and $B_s \to K$ transitions as well as forward-backward asymmetry and polarization parameters obtained in RQM agree better with lattice data than CLFQM ones. The differential distribution $d{\rm Br}(B \to \pi \mu \nu_\mu)/dq^2$ in RQM is also in better agreement with averaged experimental data, however the present experimental accuracy is not enough to distinguish between models. It is found that some forward-backward asymmetry and polarization parameters substantially differ in considered models and some of them have even opposite signs. Such phenomenon also occurs frequently in nuclear physics—results of spin observables can be quite different in different models while the total cross sections agree rather well. The most sensitive observables were identified. Thus their measurement can help to discriminate between models and determine the q^2 dependence of the form factors. From a more recent and realistic perspective, one could measure $A_{\rm FB}(q^2)$ and $C_F^\ell(q^2)$ as a first step, which is feasible through an analysis to the two-dimensional $(q^2, \cos\theta)$ distribution of event number with a large-statistics data. Actually we need to go beyond the measurement of an absolute branching fraction.

ACKNOWLEDGMENTS

We are grateful to D. Ebert and M. Ivanov for valuable discussions. The author X. W. K. acknowledges the support from the National Natural Science Foundation of China (NSFC) under Project No. 11805012.

[1] R. L. Workman *et al.* (Particle Data Group), Review of particle physics, Prog. Theor. Exp. Phys. **2022**, 083C01 (2022).
[2] P. Gambino, A. S. Kronfeld, M. Rotondo, C. Schwanda, F. Bernlochner, A. Bharucha, C. Bozzi, M. Calvi, L. Cao, G. Ciezarek *et al.*, Challenges in semileptonic B decays, Eur. Phys. J. C **80**, 966 (2020).
[3] F. U. Bernlochner, M. F. Sevilla, D. J. Robinson, and G. Wormser, Semitauonic b-hadron decays: A lepton flavor universality laboratory, Rev. Mod. Phys. **94**, 015003 (2022).

[4] P. Ball and R. Zwicky, New results on $B \to \pi, K, \eta$ decay form factors from light-cone sum rules, Phys. Rev. D **71**, 014015 (2005).

[5] O. Witzel, Lattice QCD (focus on Charm and Beauty form factors, $R(D^*)$, b- \ & c-quark masses), Proc. Sci., Beauty2019 (**2020**) 037 [arXiv:2002.01056].

[6] O. Heger, M. Gómez-Rocha, and W. Schweiger, Weak transition form factors of heavy-light pseudoscalar mesons for space- and timelike momentum transfers, Phys. Rev. D **104**, 116005 (2021).

[7] H. Zhou, Q. Yu, X. C. Zheng, H. B. Fu, and X. G. Wu, A new determination of $|V_{cb}|$ using the three-loop QCD corrections for the $B \to D^*$ semi-leptonic decays, arXiv:2206.02503.

[8] H. Y. Xing, Z. N. Xu, Z. F. Cui, C. D. Roberts, and C. Xu, Heavy + heavy and heavy + light pseudoscalar to vector semileptonic transitions, arXiv:2205.13642.

[9] R. N. Faustov, V. O. Galkin, and X. W. Kang, Semileptonic decays of D and D_s mesons in the relativistic quark model, Phys. Rev. D **101**, 013004 (2020).

[10] R. C. Verma, Decay constants and form factors of s-wave and p-wave mesons in the covariant light-front quark model, J. Phys. G **39**, 025005 (2012).

[11] L. Zhang, X. W. Kang, X. H. Guo, L. Y. Dai, T. Luo, and C. Wang, A comprehensive study on the semileptonic decay of heavy flavor mesons, J. High Energy Phys. 02 (2021) 179.

[12] D. Ebert, R. N. Faustov, and V. O. Galkin, Properties of heavy quarkonia and B_c mesons in the relativistic quark model, Phys. Rev. D **67**, 014027 (2003).

[13] D. Ebert, R. N. Faustov, and V. O. Galkin, Mass spectra and Regge trajectories of light mesons in the relativistic quark model, Phys. Rev. D **79**, 114029 (2009).

[14] D. Ebert, R. N. Faustov, and V. O. Galkin, Heavy-light meson spectroscopy and Regge trajectories in the relativistic quark model, Eur. Phys. J. C **66**, 197 (2010).

[15] D. Ebert, R. N. Faustov, and V. O. Galkin, Spectroscopy and Regge trajectories of heavy quarkonia and B_c mesons, Eur. Phys. J. C **71**, 1825 (2011).

[16] D. Ebert, R. N. Faustov, and V. O. Galkin, Analysis of semileptonic B decays in the relativistic quark model, Phys. Rev. D **75**, 074008 (2007).

[17] R. N. Faustov and V. O. Galkin, Weak decays of B_s mesons to D_s mesons in the relativistic quark model, Phys. Rev. D **87**, 034033 (2013).

[18] R. N. Faustov and V. O. Galkin, Charmless weak B_s decays in the relativistic quark model, Phys. Rev. D **87**, 094028 (2013).

[19] D. Ebert, R. N. Faustov, and V. O. Galkin, Weak decays of the B_c meson to charmonium and D mesons in the relativistic quark model, Phys. Rev. D **68**, 094020 (2003); Weak decays of the B_c meson to B_s and B mesons in the relativistic quark model, Eur. Phys. J. C **32**, 29 (2003).

[20] R. N. Faustov and V. O. Galkin, Heavy quark $1/m_Q$ expansion of meson weak decay form-factors in the relativistic quark model, Z. Phys. C **66**, 119 (1995).

[21] M. A. Ivanov, J. G. Körner, J. N. Pandya, P. Santorelli, N. R. Soni, and C. T. Tran, Exclusive semileptonic decays of D and D_s mesons in the covariant confining quark model, Front. Phys. (Beijing) **14**, 64401 (2019); M. A. Ivanov, J. G. Körner, and C. T. Tran, Exclusive decays $B \to \ell^- \bar{\nu}$ and $B \to D^{(*)} \ell^- \bar{\nu}$ in the covariant quark model, Phys. Rev. D **92**, 114022 (2015).

[22] A. Bazavov *et al.* (Fermilab Lattice and MILC Collaborations), Semileptonic form factors for $B \to D^* \ell \nu$ at nonzero recoil from 2 + 1-flavor lattice QCD, arXiv:2105.14019.

[23] E. McLean, C. T. H. Davies, J. Koponen, and A. T. Lytle, $B_s \to D_s \ell \nu$ form factors for the full q^2 range from lattice QCD with non-perturbatively normalized currents, Phys. Rev. D **101**, 074513 (2020).

[24] J. Harrison and C. T. H. Davies (LATTICE-HPQCD Collaboration), $B_s \to D_s^*$ form factors for the full q^2 range from lattice QCD, Phys. Rev. D **105**, 094506 (2022).

[25] G. Martinelli, M. Naviglio, S. Simula, and L. Vittorio, $|V_{cb}|$, lepton flavour universality and $SU(3)_F$ symmetry breaking in semileptonic $B_s \to D_s^{(*)} \ell \nu_\ell$ decays through unitarity and lattice QCD, arXiv:2204.05925.

[26] J. Harrison, C. T. H. Davies, and A. Lytle (HPQCD Collaboration), $B_c \to J/\psi$ form factors for the full q^2 range from lattice QCD, Phys. Rev. D **102**, 094518 (2020); L. J. Cooper, C. T. H. Davies, and M. Wingate (HPQCD Collaboration), Form factors for the processes $B_c^+ \to D^0 \ell^+ \nu_\ell$ and $B_c^+ \to D_s^+ \ell^+ \ell^+ (\nu \bar{\nu})$ from lattice QCD, Phys. Rev. D **105**, 014503 (2022).

[27] E. Dalgic, A. Gray, M. Wingate, C. T. H. Davies, G. P. Lepage, and J. Shigemitsu, B meson semileptonic form-factors from unquenched lattice QCD, Phys. Rev. D **73**, 074502 (2006); **75**, 119906(E) (2007).

[28] M. Okamoto, C. Aubin, C. Bernard, C. E. DeTar, M. Di Pierro, A. X. El-Khadra, S. Gottlieb, E. B. Gregory, U. M. Heller, J. Hetrick *et al.*, Semileptonic $D \to \pi/K$ and $B \to \pi/D$ decays in 2 + 1 flavor lattice QCD, Nucl. Phys. B, Proc. Suppl. **140**, 461 (2005).

[29] J. A. Bailey, C. Bernard, C. E. DeTar, M. Di Pierro, A. X. El-Khadra, R. T. Evans, E. D. Freeland, E. Gamiz, S. Gottlieb, U. M. Heller *et al.*, The $B \to \pi \ell \nu$ semileptonic form factor from three-flavor lattice QCD: A model-independent determination of $|V_{ub}|$, Phys. Rev. D **79**, 054507 (2009).

[30] J. M. Flynn, T. Izubuchi, T. Kawanai, C. Lehner, A. Soni, R. S. Van de Water, and O. Witzel, $B \to \pi \ell \nu$ and $B_s \to K \ell \nu$ form factors and $|V_{ub}|$ from 2 + 1-flavor lattice QCD with domain-wall light quarks and relativistic heavy quarks, Phys. Rev. D **91**, 074510 (2015).

[31] B. Colquhoun *et al.* (JLQCD Collaboration), Form factors of $B \to \pi \ell \nu$ and a determination of $|V_{ub}|$ with Möbius domain-wall-fermions, arXiv:2203.04938.

[32] G. Martinelli, S. Simula, and L. Vittorio, Exclusive semileptonic $B \to \pi \ell \nu_\ell$ and $B_s \to K \ell \nu_\ell$ decays through unitarity and lattice QCD, arXiv:2202.10285.

[33] C. M. Bouchard, G. P. Lepage, C. Monahan, H. Na, and J. Shigemitsu, $B_s \to K \ell \nu$ form factors from lattice QCD, Phys. Rev. D **90**, 054506 (2014).

[34] A. Bazavov *et al.* (Fermilab Lattice and MILC Collaborations), $B_s \to K \ell \nu$ decay from lattice QCD, Phys. Rev. D **100**, 034501 (2019).

[35] W. Jaus, Semileptonic decays of B and d mesons in the light front formalism, Phys. Rev. D **41**, 3394 (1990); Relativistic constituent quark model of electroweak properties of light mesons, Phys. Rev. D **44**, 2851 (1991).

[36] G. P. Lepage and S. J. Brodsky, Exclusive processes in perturbative quantum chromodynamics, Phys. Rev. D **22**, 2157 (1980).

[37] H. Ha *et al.* (Belle Collaboration), Measurement of the decay $B^0 \to \pi^- \ell^+ \nu$ and determination of $|V_{ub}|$, Phys. Rev. D **83**, 071101 (2011).

[38] A. Sibidanov *et al.* (Belle Collaboration), Study of exclusive $B \to X_u \ell \nu$ decays and extraction of $\|V_{ub}\|$ using full reconstruction tagging at the Belle experiment, Phys. Rev. D **88**, 032005 (2013).

[39] J. P. Lees *et al.* (BABAR Collaboration), Branching fraction and form-factor shape measurements of exclusive charmless semileptonic B decays, and determination of $|V_{ub}|$, Phys. Rev. D **86**, 092004 (2012).

[40] Y. S. Amhis *et al.* (HFLAV Collaboration), Averages of b-hadron, c-hadron, and τ-lepton properties as of 2021, arXiv:2206.07501.

[41] A. Abdesselam *et al.* (Belle Collaboration), Measurement of the D^{*-} polarization in the decay $B^0 \to D^{*-} \tau^+ \nu_\tau$, arXiv:1903.03102.

[42] S. Hirose *et al.* (Belle Collaboration), Measurement of the τ Lepton Polarization and $R(D^*)$ in the Decay $\bar{B} \to D^* \tau^- \bar{\nu}_\tau$, Phys. Rev. Lett. **118**, 211801 (2017).